PNAS Nexus, 2024, 3, pgae495
https://doi.org/10.1093/pnasnexus/pgae495
Advance access publication 3 December 2024
Research Report

Design and fabrication of a parasite-inspired, millimeter-scale tissue anchoring mechanism

Gabriel Maquignaz[a,b], Rachel Zoll[a], Michael Karpelson[a], James C. Weaver[a,c,*] and Robert J. Wood[a,*]

[a]Harvard John A. Paulson School of Engineering and Applied Science, Harvard University, Cambridge, MA 02139, USA
[b]École Polytechnique Fédérale de Lausanne (EPFL), Institute of Electrical and Micro Engineering, Lausanne CH-1015, Vaud, Switzerland
[c]Wyss Institute for Biologically Inspired Engineering, Harvard University, Boston, MA 02215, USA
*To whom correspondence should be addressed: Email: james.weaver@wyss.harvard.edu (J.C.W.); rjwood@seas.harvard.edu (R.J.W.)
Edited By Cristina H. Amon

Abstract

Optimizing mechanical adhesion to specific human tissue types is a field of research that has gained increasing attention over the past two decades due to its utility for diagnostics, therapeutics, and surgical device design. This is especially relevent for medical devices, which could benefit from the presence of attachment mechanisms in order to better target-specific regions of the gastrointestinal (GI) tract or other soft tissues for sensing, sample collection, and drug release. In this work, and inspired by the tissue anchoring adaptations found in diverse parasitic taxa, we present a design and manufacturing platform for the production of a nonintuitive bioinspired millimeter-scale articulated attachment mechanism using laminate fabrication techniques. The functional design closely mimics the geometry and motions of curved hooks employed by some species of tapeworms to attach to their host's intestinal walls. Here, we show the feasibility of such a mechanism both in terms of attachment capabilities and manufacturability. Successful attachment of a prototype to tissue-simulating synthetic medical hydrogels is demonstrated with an adhesion force limited only by the ultimate strength of the tissue. These results demonstrate the efficacy of parasite-inspired deployable designs as an alternative to, or complement to, existing tissue attachment mechanisms. We also describe the design and manufacturing process workflow and provide insights for scaling the design for mass-production.

Keywords: bioinspired, parasitology, tissue attachment mechanism, microfabrication

Significance Statement

Implantable and ingestible devices provide minimally invasive methods for delivering drugs, diagnosing, and monitoring previously difficult-to-detect pathologies. These devices often require tissue attachment mechanisms in order to perform tasks for extended periods of time at a target location. To meet these needs, and inspired by the structural and tissue-specific anchoring ornamentations present in diverse parasitic taxa, this paper presents a versatile research platform for the design of bioinspired attachment mechanisms using a layer-by-layer fabrication method which draws inspiration from the printed circuit board industry. This manufacturing technique produces scalable devices—both physically scalable to be used in remote locations in the body, and compatible with large-scale production, which could help advance the fields of attachable medical devices and diagnosis of soft tissue pathologies.

Introduction

Soft tissue anchoring has uses across a broad range of medical applications, from temporary tissue anchoring for sensing and treatment to assistance with manipulation of delicate tissue for minimally invasive procedures. Anchoring in place at a specific location, either briefly or for longer durations, further expands options for diagnosis and treatment. For example, implantable devices can be anchored to soft tissue in the gastrointestinal (GI) tract to monitor biometric signals including core body temperature (1), gas concentrations (2), and medication adherence (3). Anchored devices can also deliver drugs to the target tissue over an extended period of time (4), maintaining medication delivery for chronic conditions (5). Direct contact with tissue further enables continuous electrical recording and stimulation (6, 7) of stomach and bladder tissue, enhancing motility in paralyzed or impaired tissue regions. Furthermore, anchored devices can provide temporary mechanical assistance to help manipulate delicate tissue structures such as blood vessels (8) or ureters (9). Small-scale versions of these tissue-anchoring mechanisms could be integrated onto existing devices and deployed at the distal end of existing medical instruments, such as catheters, end effectors, and laparoscopes.

Mechanical interlocking-based attachment can also be used to adhere to delicate structures in nonclinical contexts (10). For example, wearable sensor tags can be applied to small or soft

Competing Interest: The authors declare no competing interests.
Received: October 2, 2024. **Accepted:** October 5, 2024

Table 1. ICR and soft tissue attachment mechanisms.

Mechanism	Actuation	Target site	Medical application	Ref.
Deployable legs	Brushless motor	Esophagus	CE	(16)
Unfoldable arms	Passive unfolding	Stomach	DD	(17)
Star-shaped unfoldable dosage forms	Passive unfolding	Stomach, Bladder	DD	(9, 18–20)
External magnetic force	Magnetic-driven	Stomach, Bladder	DD, CE, Biopsy	(9, 21–24)
Hooked probes	Loaded spring	Stomach, Bladder	DD, Electrical stimulation	(6, 25, 26)
Supra-molecular polymer gel ring	pH-induced swelling	Stomach	DD, Diagnosis	(27)
Inflatable balloon	Effervescent chemicals	Stomach	Obesity treatment	(28, 29)
Needle array and sucker	Vacuum chamber	Small intestine	DD, Biosensor deployment	(30–35)
Anchoring modules	Magnetic-driven	Small intestine	DD	(36)
Deployable adhesive legs	SMA wire	Small intestine	CE	(37, 38)
Muscular contraction	Electrical stimulus	Small intestine	CE	(39)
Curved scissor mechanism	Magnetic-driven	Small intestine	CE	(40)
Latching sharp microtips	Thermal differential stress release	Entire GI tract	DD	(41)
Soft gripping microfingers	Shape memory polymer	Blood vessel	Manipulation	(8)

Partially adapted from (1). (CE, capsule endoscopy; DD, drug delivery).

organisms, e.g. to monitor marine species and their behavioral patterns (11). In the consumer products context, easy to apply and remove temporary textile attachment mechanisms could be employed in retail anti-theft devices or for the integration of electronic components into garments (12). Additionally, these attachment mechanisms could be adapted to rapidly patch soft structures such as elastomers or fabrics.

One category of biomedical devices that can benefit from controlled adhesion with soft tissue are ingestible capsule robots (ICRs). ICRs have a number of applications in the diagnosis and treatment of various GI tract pathologies, as described in recent reviews by Mau et al. (1) and Cummins (13). These functions can be fulfilled as an ICR passively moves through the GI tract due to natural peristaltic constrictions associated with digestion. However, the ability of an ICR to remain attached at a specific location is often a key requirement for site-specific monitoring, data acquisition through biosensing for extended periods of time (14, 15), or when inspecting segments of the GI tract where the transit time is too short, like in the esophagus (16). To address these demands, significant research effort has been put into the development of tissue attachment mechanisms. A nonexhaustive list of existing tissue-attachment devices is shown in Table 1 to reflect the current state of the art.

In order to remain stationary at a specific location in the body, mechanical tissue attachment design strategies have primarily fallen into one of two categories. The first involves increasing the dimensions of the device to prevent it from moving further once the device is deployed its target location. This principle is most effective for stomach or bladder-residing devices, as the diameter of the tract decreases near the pylorus/urethra. This working principle can be achieved in a number of ways, such as via the incorporation of passively unfolding structures (17–20), inflating balloons filled with effervescent chemicals (28, 29, 42), employing swellable materials (27), and actively deploying features like adhesive legs (16, 37, 38) and anchoring modules (36, 40). This same principle can also be leveraged to achieve attachment in the intestine or the esophagus. However, because of the approximately constant diameter of the GI tract in these regions, the attachment must rely on frictional forces and deformations of the walls of the tract, which can prove challenging, in particular, due to peristalsis (1). Furthermore, this approach of relying on the diameter of the device being similar to that of the GI tract at a specific location severely limits the potential for miniaturization.

The second attachment principle is based on mechanical interlocking with the walls of the soft tissue. This approach relies on the presence of sharp features for perforating the mucosa and the first few layers of tissue to anchor the device at the desired location (43, 44). In order to accommodate these needs, the diverse tissue anchoring ornamentations found in parasitic taxa offer a wealth of design inspirations (Fig. 1). Encompassing a wide range of highly specialized hook and sucker geometries, including both spatially segregated and functionally integrated configurations, this vast array of holdfast structures have evolved to function across a variety of habitats (colonizing both aquatic, and terrestrial hosts), and exhibit specialized modifications that are adapted for anchoring into substrates with diverse moduli and surface textures (54). Furthermore, these parasitic taxa also span a wide range of different length scales, and are adapted for survival across an equally broad range of Reynold's numbers. Since many of these species exhibit high host- or tissue-type specificity (55–57), these substrate anchoring modifications thus offer a rich bioinspired, and application-specific design space for the development of their engineered analogs. These engineered analogs could also be used as a platform to study the role of different attachment organ geometries in tissue irritation and host pathology. Previous examples of these bioinspired ICR tissue anchoring geometries include sucker-coupled circular needle arrays (30–35), and simple spring-loaded probes with hooked tips (6), inspired by tapeworms and lampreys, and small micromechanical grippers inspired by hookworm jaws (41) (cf. Fig. 1). Swellable microneedle arrays inspired by the attachment organs of acanthocephalan endoparasites (cf. Fig. 1) have also been demonstrated (58), but not for ICR attachment. In terms of broad ranging applicability, these approaches are more universal in the sense that they do not rely on the shape of the GI tract at the targeted site to achieve successful attachment.

Although the high-level attachment principles of parasites like *Taenia solium* (Fig. 2A) have inspired many of these designs, the actual curved shape of its hooks and the characteristic rotating protraction motion generated by its associated musculature has never been faithfully replicated in a synthetic engineered analog, due to its complexity. Despite these apparent fabrication-related design limitations, such parasites achieve long-term adhesion while requiring only a small hook penetration depth, thus representing desirable characteristics for an attachment mechanism to reduce the risk of pain, bleeding, lasting tissue damage, and even perforation associated with deeper penetration. A subcentimeter size, integrated actuation system capable of generating fast (i.e. >100 mm/s) penetration of typical GI tract tissues, with a maximum penetration depth of 1 mm, are all desirable

characteristics for a device aimed at reproducing such an attachment strategy, especially since high penetration velocity reduces rupture deformation and work (61).

To address these current design, kinematic, and manufacturing challenges, we present an integrated workflow for the creation of a tissue attachment mechanism (TAM) based on curved hooks and a circular protraction motion inspired by the morphology of the tapeworm (*Taenia solium*) scolex (Fig. 2A). The proposed mechanism is bistable (Fig. 2B) and designed to be passively triggered when it collides with a wall of the GI tracte with a suitable orientation and sufficient force. The manufacturing of such structures is achieved using laminate fabrication techniques (62–65), which also make our design highly scalable (62), and mass-producible (63). The goal of this work is a proof of concept for such mechanisms, and to potentially pave the way for smaller, stronger, and cheaper attachment mechanisms for minimally invasive, multi-site pathology diagnosis and drug delivery.

Mechanism design and fabrication

The desired motion of each individual hook is a protraction motion constrained to a plane. The circular symmetry of the target mechanism (Fig. 2C) makes it natural to rely on a circular repetition of planar mechanisms.

Hook morphology

The hook morphology can be simplified into a two-dimensional (2D) profile (Fig. 2B). The neutral axis is a circular arc that slides along a fixed circular path as the rigid link rotates. This combination of shape and trajectory results in minimum tissue damage and penetration force since the rest of the hook follows the path of the tip and does not tear any additional tissue. The hooks are linearly tapered along the circular arc, which is equivalent to using two Archimedean spirals to define the edges (Fig. 2B). While in the present study we copied the gross geometric features of tapeworm hooks and designed the kinematics and hook arc shape to be consistent so as to minimize tissue tearing upon deployment, there are several additional aspects of hook design that could be further explored in future investigations to enhance adhesion. These parameters include the number of hooks (limited spatially), hook size, hook materials (e.g. stiffer materials that could enable thinner hooks), aditional geometric features such as barbs, and surface coatings to lubricate or promote bonding.

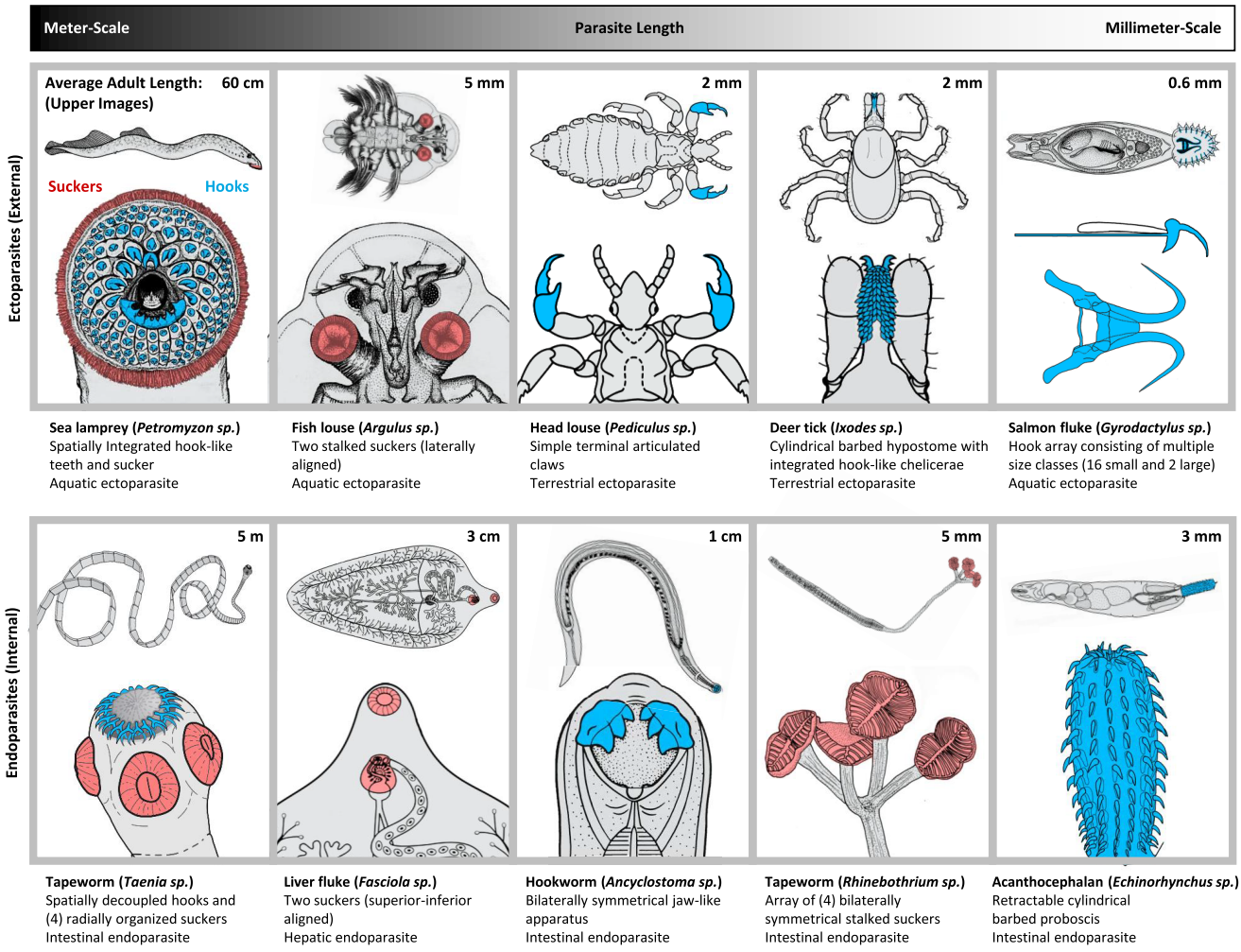

Fig. 1. Holdfast structural diversity across a wide range of parasitic taxa, which includes ecto- (upper) and endo-parasites (lower) that inhabit terrestrial or aquatic environments, and span dimensions covering nearly four orders of magnitude (from sub-millimeter to multiple meters in body length). For each species, suckers are highlighted in red, and hooks, spines, and tooth-like elements in blue. For each panel, an image of the entire parasite is shown, along with a detailed view of its attachment organ. Images adapted and redrawn from (45–53).

Planar mechanism

The first constraint for this mechanism is the target path of the hook discussed in subsection 'Hook morphology'. A circular path is easily achieved by rigidly fixing the hook to one link of a kinematic chain (adjacent to the mechanical ground) which becomes the output link of the mechanism. A second constraint is bistability, which enables storage and release of elastic potential energy, resulting in rapid, and high-force substrate penetration. Finally, a third constraint is the mechanical coupling of the output linkages to achieve synchronous deployment of all the hooks. Indeed, in the case where some hooks contact the tissue surface before others, the net reaction torque on the mechanism body is non-zero, making it rotate away from the surface and preventing the remaining hooks from penetrating the tissue.

The planar mechanism used as a building block for the complete mechanism is symmetric, is responsible for both the actuation and coupling of opposing pairs of hooks, and is made up of two output links (noted $h_{1,2}$ in Fig. 2B)—one for each hook—connected by a three-link kinematic chain.

Without additional constraints, the planar mechanism would be equivalent to a symmetric six-bar closed kinematic chain. Such a mechanism can be shown to have three degrees of freedom (DOF) using the mobility formula for planar mechanisms (66) and would not act as a coupler. By constraining the central platform (noted p in Fig. 2B) to remain horizontal and on a vertical path coincident with the axis of symmetry of the mechanism (Fig. 2B), the number of DOFs of the mechanism is reduced to one. In this work, the three-link kinematic chain comprised of a central platform with such properties and two identical lateral links (noted $s_{1,2}$ in Fig. 2B [2D Kinematic model]) is referred to as a Sarrus bridge. This configuration has the effect of coupling the rotation motions of the two output links, forcing the angles formed by the two

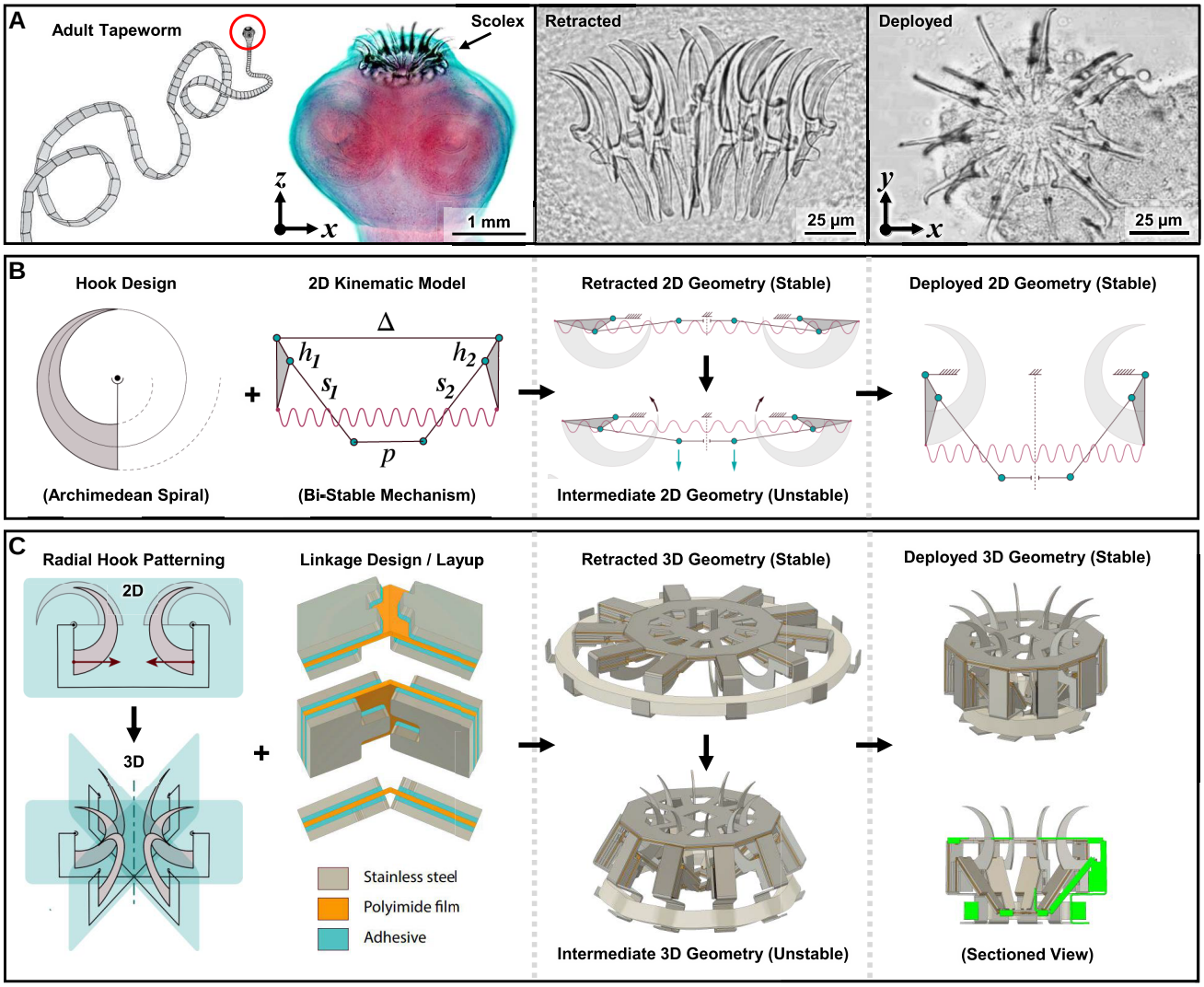

Fig. 2. Motivation and design workflow for our tapeworm-inspired tissue anchoring mechanism. A) Biological Inspiration: Hooked scolex of *Taenia solium* seen partially deployed, as well as a magnified view of both a retracted and deployed hook array in a related species (reproduced with permission from (59, 60)). A coordinate system is included to help orient the reader. B) Kinematic Modeling: Simplified hook geometry attached to a bistable kinematic linkage system, which can rotate around a fixed hinge joint. The actuation forces come from a linear elastic element shown in red. C) Functional Device Design: The 2D hook design can be patterned in a radial array, and, when combined with laminate-based manufacturing methods, can result in a fully functional three-dimensional (3D) mechanism mimicking the crown-like arrangement of hooks found in a tapeworm scolex. The final bistable 3D geometry is shown in its retracted/armed (stable), intermediate (unstable), and deployed (stable) geometries, as well as in a sectioned view (with the cutting plane location denoted in green). For all subsequent images of the devices shown in the remaining figures, the device's retracted/armed geometry measures 9.5 mm in diameter, and the deployed geometry measures 4.8 mm in diameter.

output links $h_{1,2}$ and the ground link Δ to be equal at all times. However, the coupling effect of the Sarrus bridge is lost if the mechanism is used past the kinematic singularity where the links h_1 and s_1 and h_2 and s_2 are collinear, respectively (Fig. 2B [2D Kinematic model]).

The Sarrus bridge is also key for making the mechanism bistable once a linear elastic element is added to the mechanism (shown in red in Fig. 2B). The mechanism has an "armed" (retracted) stable state and a "deployed" stable state in which the hooks are, respectively, retracted and deployed. The transition from one state to another is illustrated in Fig. 2B, with an over-centering configuration when links s_1, p, and s_2 are collinear. Triggering occurs when a sufficient external force is applied to the platform (e.g. during contact with the GI tract wall) to overcome the local energy minimum associated with the armed state. The required triggering force can be tuned by utilizing the ground link Δ as an end stop for the platform (Fig. 2B) and adjusting how far the platform is allowed to move before being blocked by the ground link when in the armed state. The closer the resting position of the platform is to the over-centering point, the smaller the required triggering force.

Complete mechanism

The complete mechanism is obtained by circular repetition of N planar mechanisms as described in subsection 'Planar mechanism' and has $2N$ hooks. The planar mechanisms share common ground links and platform links (respectively, noted Δ and p in Fig. 2B). This design makes the complete mechanism a variation of a Sarrus linkage (67), and has the effect of constraining the central platform to remain parallel to the ground platform and to follow a linear vertical trajectory as required by each individual planar mechanism. In addition, the linear elastic element is implemented using a ring-like elastic element placed around the mechanism as shown in Fig. 2C.

The final prototype is shown in Fig. 2C. It is composed of $N = 5$ planar mechanisms and has vertical spokes attached to the central platform that poke out when the mechanism is armed (cf. Fig. 2C, Retracted 3D Geometry). These spokes are used as an example triggering method which could be replaced with an actuator in future work. They transfer external forces to the platform and thus trigger the mechanism when they interact with a surface. The device is made from stainless steel and polyimide film using laminate manufacturing, and the hinges are implemented using castellated flexure joints (63, 68) (Fig. 2C, Linkage Design).

To maximize the penetration force and adhesion capabilities, the version of the mechanism presented in this work is designed for single triggering and cannot be rearmed. Once deployed, the elastic element is too strong for the mechanism to be reverted to its armed state (cf. Fig. 2B, Retracted 3D Geometry) without exceeding the ultimate strength of the hinges in the process. Despite the lack of mechanism reversibility in the current design, this device could detach passively after a certain period of time, as it slowly pulls through the adjacent tissue, as has been demonstrated for other fixed-needle devices (30–35).

Manufacturing

The mechanism was constructed using laminate manufacturing (62–65, 68) techniques. The rigid links, plates, and hooks are made of stainless steel, the hinges are made of polyimide film, and all layers were bonded together using Pyralux adhesive layers. The steel, polyimide, and adhesive layers are 50.8 μm, 25.0 μm, and 25.4 μm thick, respectively.

The layers were first laser-cut (Fig. 3A) while leaving small temporary bridges along the pattern contour to connect the device to the rest of the layer until the bonding step (cf. Fig. S2). After removing the scraps, each layer was cleaned in an ultrasonic bath with water and detergent.

Adhesive layers on the backing paper were laser-patterned to remove adhesive where it was not needed, precisely aligned with the corresponding layer using high-tolerance alignment pins, and tacked onto the back of each layer using a heat press (cf. Fig. S3). The tacked layers were then aligned again following the same principle, and bonded in a heat press. In some places, to ensure proper pressure transfer from the top plate to the bottom plate of the press (and thus proper adhesion), sub-assembly stacks were first bonded separately, and then subsequently bonded to the rest of the stack. An illustration of each individual layer is provided in Fig. S1.

The design contained elements that are out of the horizontal plane, and must be first cut in-plane before being folded out of plane (Fig. 3A). This was the case for the hooks, the retaining features for the elastic element at the end of each arm, and the two triggering spokes (cf. Fig. 2C, Retracted 3D Geometry). These features were first released by cutting the bridges that prevented them from folding out of plane during earlier steps (Fig. 3B), and were then bent and formed into their final shape using a modeling knife and fine tweezers (cf. Fig. S4). While this process is delicate and time-consuming, it could easily be automated and made more repeatable by designing folding dies with alignment holes.

After the out-of-plane features were folded, the rest of the bridges were cut, and the device was released from the layer stack, which was discarded. The last step was the mounting of the elastic element. Elastic elements were cut in batches from 400 μm thick durometer 30A silicone sheets (Fig. 3B, Final Assembly), and were then mounted on the device using a thick-walled polyimide tube as a stent (cf. Fig. S5). The device was placed on one end of the tube in its armed state, and the elastic element was slid along the polyimide tube until it naturally sat in the retaining features, at which point the tube could be removed (Fig. 3B, Final Assembly). The mechanism is now armed and ready to be deployed. In a final device, one last bending step would consist of closing the retaining features around the elastic element to lock it in place. In this work, however, the retaining features were left open for practical reasons, and as such, this version of the mechanism cannot be re-armed (cf. subsection 'Complete mechanism'). Therefore, leaving the retaining features open allowed for the removal of the elastic element after a prototype was triggered, without interfering with the proper functioning of the mechanism. The mechanism is then manually reverted to its armed state, and a new elastic element can be installed (Fig. 3B, Final Assembly). By using this approach, each prototype is reusable for additional experiments as long as it remains undamaged.

Results

The final, fully-assembled design presented in this work is shown in (Fig. 3C). It measures 9.5 mm and 4.8 mm in diameter when in its armed and deployed states, respectively, and weighs 44 mg. The hooks measure 50.8 μm thick and have an arc radius (Fig. 3C) of 1 mm. The widest part of a hook is 496 μm wide, which makes it similar in dimensions to the tip of a 25 G standard hypodermic needle (500 μm width). Additional SEM images are shown in Fig. S6. The smallest adhesive bonding pads between layers of steel and polyimide have a surface area of 0.36 mm^2. Based on the chosen manufacturing process, this device scale proved to

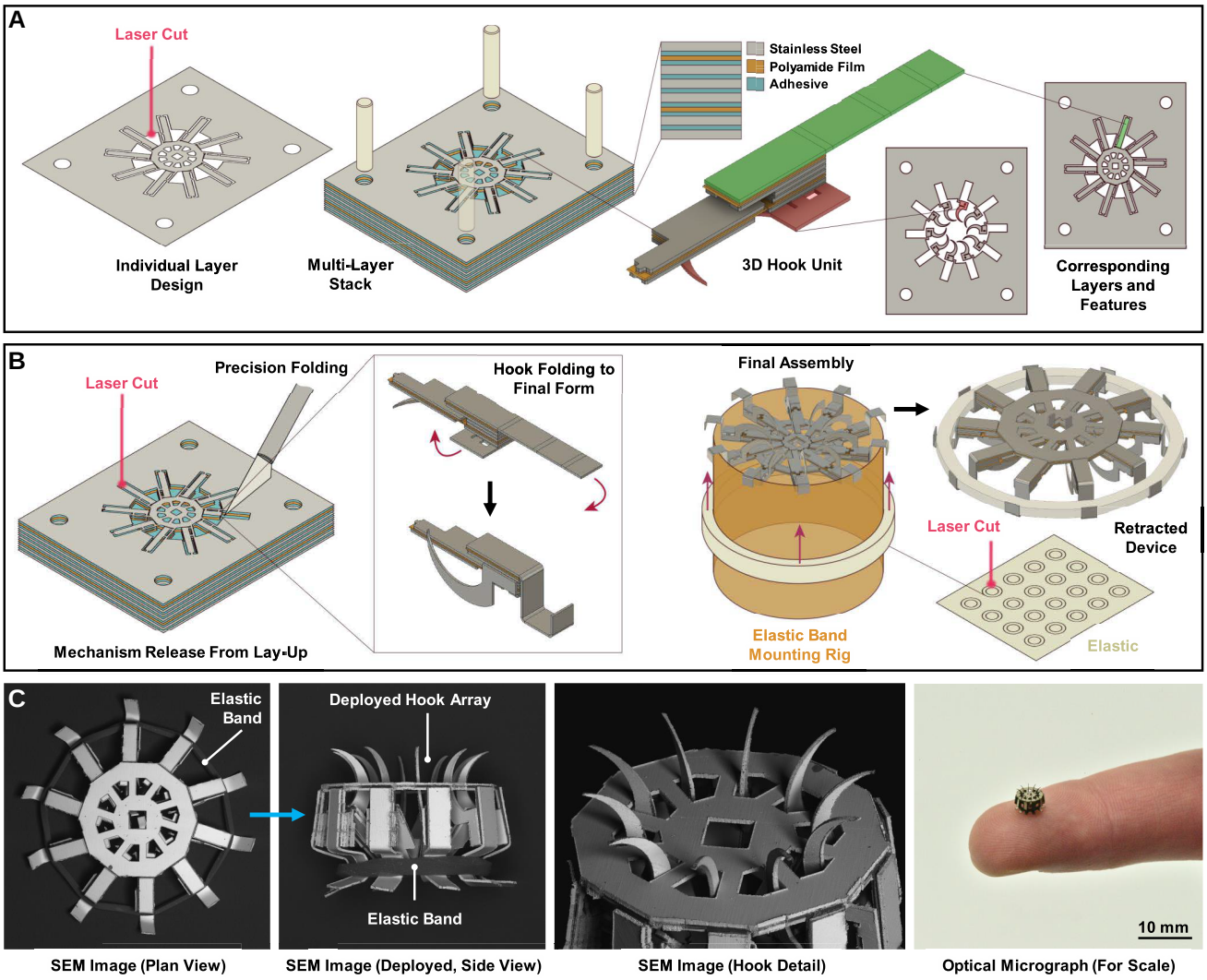

Fig. 3. Multistep laminate manufacturing of the functional bistable mechanism. A) Individual layers are laser-cut, and tooling holes are added for future alignment purposes. The layers are then stacked and aligned using high-tolerance alignment pins and bonded in a heat press. The hooks and retaining features for the elastic element are first manufactured in-plane and bonded to the rest of the device. B) Laser cuts are made to release the features that need to be bent. The features are then bent manually out-of-plane using a small hobby knife and precision tweezers. Each hook is folded sideways into the plane of the linkage it is attached to, the straight beam bonded to the top layer is shaped into a retaining feature, and the two spokes attached to the central platform are bent upwards so that they protrude from the ground link when the mechanism is armed. After fully releasing the device, the elastic band-like element (which was laser-cut from a 400 μm thick durometer 30A silicone sheet) is mounted on the device in its armed state using a tube made of thick polyimide film as a stent. C) Scanning electron micrographs of the fully assembled mechanism shown in both retracted (fully armed) and deployed configurations. The hook assembly is shown in detail as well as an accompanying optical photograph of the same model, with a finger for scale.

be the smallest that could be reproducibly manufactured using the chosen adhesive due to delamination issues when smaller geometries of bonding pads were explored.

Humimic Medical hydrogel blocks mimicking the mechanical properties of soft tissue were used to evaluate device performance (69, 70). The device was first placed on the surface of a gel block in its armed state and manually triggered by applying a short burst of downward force on the arms (Fig. 4A, B). The average observed peak force required to trigger the mechanism across five trials on the same device was approximately 5.7 N (Fig. 4C). The device reliably worked as intended, with the hooks deploying and penetrating the surface of the gel in less than a millisecond (Fig. 4C), anchoring the mechanism to the block. A nylon cable was then used to pull the device upward to conduct a detachment test using a single-column Instron pull-tester (Fig. 4D, upper photograph). The adhesion force of four nominally identical devices was evaluated with three separate trials per device ($n = 12$ total tests). The resulting force–displacement curves were then aligned according to the steep drop in force corresponding to complete detachment from the block, using the minimum of the first derivative, to allow for the computation of the average curve shown in Fig. 4D.

Finally, after the pulling-induced detachment of the device, the resulting damage to the gel block could be assessed (Fig. 4D, lower photograph). The hooks tore through the hydrogel block along a vertical trajectory on their way out of the block as expected. However, while the hydrogel was designed to mimic the stiffness and resistance to surface puncture of human soft tissue, the damage to the hydrogel takes the form of brittle fracture, which is not representative of the behavior of living tissue when subjected to a similar loading regime. While local crack propagation collinear to the hook extraction path is expected (61), cracks also propagated perpendicularly to the detachment path of the hook and relatively far away from the location of crack initiation. These cracks do not

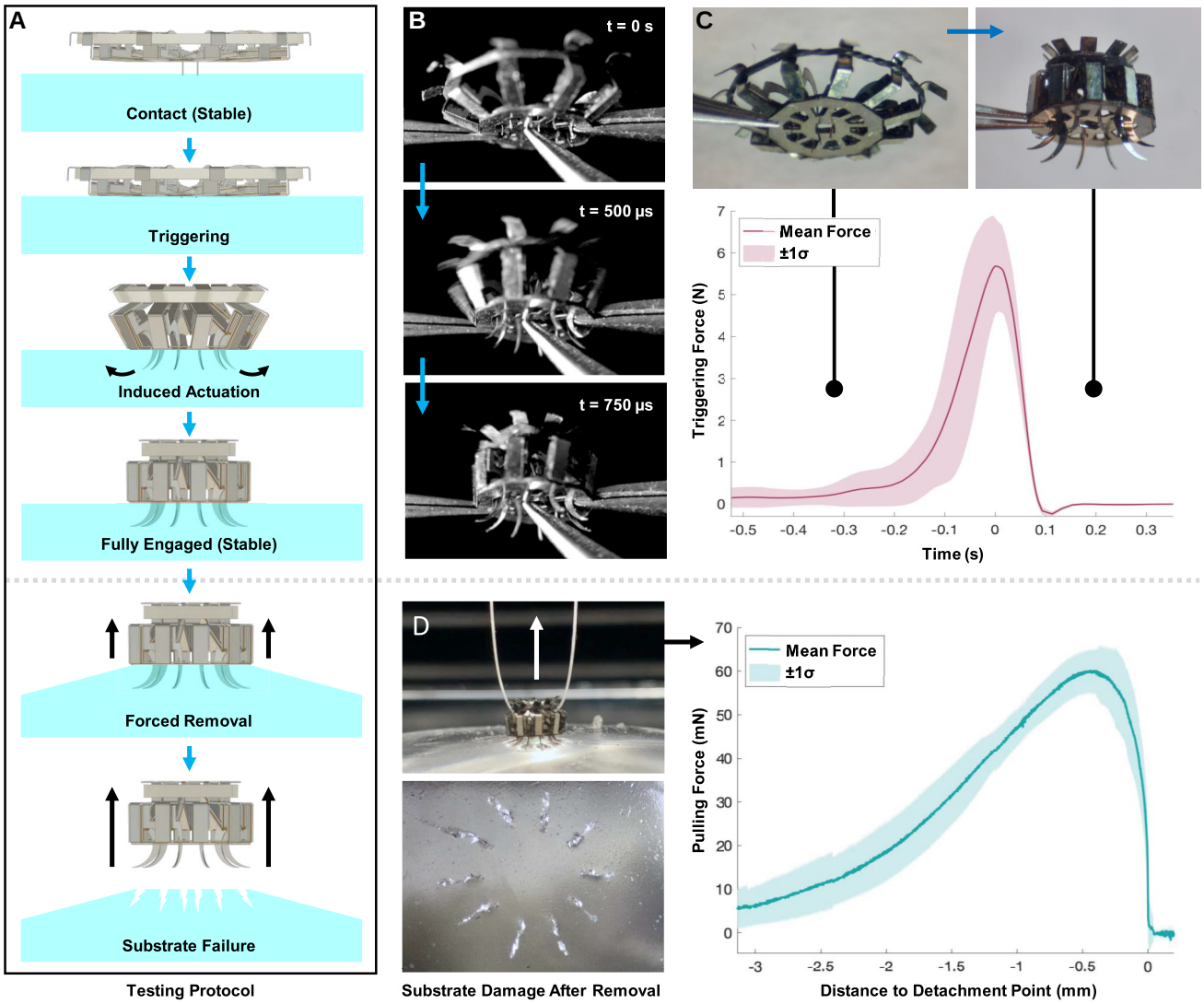

Fig. 4. Device performance testing. A) An overview of our experimental testing protocol, which consists of six distinct steps: substrate contact, triggering, induced actuation, and engagement, followed by pull-off, and subsequent substrate structural failure. The tissue-mimicking hydrogel substrate is indicated in blue. B) Screenshots from a high-speed video of a device being triggered. The triggering is performed using a pair of fine pliers to exert a force on the triggering spokes. The video was recorded at 8,000 fps, and three different time frames are displayed. The time $t = 0$ was set to be the instant when the over-centering point between the two stable states of the mechanism was reached. C) Plot showing mean triggering force as a function of time, averaged over five different tests, with the shaded region corresponding to ± one standard deviation. Photographs of the retracted and deployed devices are displayed, in relation to their relative time points during the performed test. D) Following device triggering into a hydrogel substrate (upper photograph), the device was pulled away using the attached nylon cable (shown in white) until substrate failure occurred (lower photograph). The corresponding graph plotting mean pulling force as a function of distance to the detachment point is shown, averaged over three different tests performed on each of four different devices (total tests $n = 12$), with the shaded region corresponding to ± 1 SD. The large drop at −0.5 mm corresponds to the point at which substrate failure began to occur.

accurately reflect the amount of tearing expected in natural tissue. In addition, increasing the thickness of the hooks to make them more blunt—thus theoretically increasing the force necessary to cut through tissue and detach—had no significant effect when tested on hydrogel blocks. This observation may simply be due to the brittle failure mode of the hydrogel material, where the detachment process involved long-distance crack propagation until it reached the hydrogel surface, rather than reaching a high compressive stress to cut the gel, as would be more representative of real biological tissue.

Discussion

The tapeworm-inspired deployable adhesion mechanism presented in this work was shown to perform as intended. In particular, the nonlinear kinematic behavior produced a fast, synchronized outward rotational deployment of the hooks, resulting in repeatable attachment to tissue-simulating medical hydrogels. When a sufficient vertical force is applied to the mechanism (Fig. 4D, upper photograph), the hooks penetrate the tissue, demonstrating that the elastic element (coupled through the bistable kinematic mechanism) is sufficiently strong to ensure the mechanism is nonback-drivable over the range of forces of interest. Moreover, except for brittle fracture observed in hydrogel testing blocks, the mechanism only damaged a small amount of tissue as it was retracted, as expected.

In future studies, the device could be further miniaturized to allow for efficient integration into surgical devices and reduced tissue damage. However, the current device dimensions are sufficiently close to those commonly employed in ICRs (13),

demonstrating that the design and manufacturing techniques presented here represent a viable option. While in future designs, the size of the hooks (relative to the device size) could be independently modified, it should be noted that there exists a tradeoff between increasing the adhesion capabilities with deeper hook penetration and minimizing tissue damage with shallower hooks. Additional investigations aimed at exploring these tradeoffs would highly benefit from further exploration of tissue-specific holdfast architectures found in other parasitic taxa (cf. Fig. 1), while simultaneously taking into consideration their associated attachment-related host pathologies.

The average peak force required to trigger the mechanism was approximately 5.7 N (Fig. 4C). This force magnitude is due to manufacturing tolerances at the joints and unwanted deflection of the rigid links, resulting in a modified equilibrium position and thus dramatically increasing the height of the energy barrier to be overcome. This can be observed by visually comparing the theoretical (Fig. 4A, Contact [Stable]) and observed (Fig. 4C [left]) armed equilibrium positions.

While the mechanism and its general working principle are viable at this size scale, these results show the need for more advanced triggering methods and increased tolerances and reliability in the manufacturing process. Chemical methods such as soluble adhesives or pH-based inflatable triggers could be good candidates for this application. Electronic options such as fuse-based or shape-memory alloy-based electrothermal or electromagnet-based triggering could also be investigated since these methods would provide further control over deployment timing.

The observed average detachment force of approximately 60 mN corresponds to the specific resistance-to-cutting of the hydrogel used for testing and will differ for other tissues and hook morphologies. While the current smooth hook morphology in our fabricated devices was specifically chosen to replicate hook geometries found in living tapeworms, it should be noted that hook morphology likely has a substantial impact on the tearing force in real tissue, and thus on the adhesion performance of the device. Since tapeworms have the ability to move throughout their host's GI tract, smooth hooks make sense from a reversibility perspective.

This device could also be used as a platform to investigate the role of different parasite attachment organ geometries in tissue irritation and host pathology, providing a path forward for the development of medical devices with reduced patient morbidities. While this work explores one initial set of hook geometries, the hook design space could be further expanded to study additional features such as the width, length, height, and insertion angle of the hooks. Furthermore, additional hook geometries could incorporate barbed edges similar to those found in bee stingers (71), and other more permanent substrate anchoring geometries depending on the intended medical applications.

For example, adding anchoring capabilities to existing ICR platforms could enable new types of treatment. Diagnosis methods for ICRs already include imaging with optical (72, 73) or ultrasound sensors (74, 75), monitoring pH (76, 77), pressure (78, 79), and temperature (1), as well as detecting chemical (80) and biological (81) changes. From a therapeutic perspective, ICRs can be used to deliver long-acting small molecule drugs or biologics to improve medication adherence (1, 82), or when standard oral delivery is not possible (30, 31, 83). They could also be used to deliver electrical stimulation via the hooks. By combining multiple sensing and treatment modalities, anchored ICRs could thus offer many additional diagnostic and therapeutic capabilities.

While in-house prototype production is time-consuming due to multiple manual assembly operations that are not practical to automate in an academic lab setting, the manufacturing process is inherently highly scalable (63). This work also demonstrates a new process within the framework of laminate manufacturing: the bending of fine steel features to achieve high aspect ratio 3D structures. In a high-volume manufacturing scenario, such bending operations could be automated through precision forming dies with appropriately positioned features. This approach would allow for simultaneous bending of all instances of a desired feature (e.g. all hooks) in a press, significantly increasing the efficiency, accuracy, and repeatability of the manufacturing process. In addition, laminate manufacturing has been shown to be compatible with a large array of biocompatible medical-grade materials and adhesives (65), further illustrating the real-world utility of these devices in a therapeutic context.

Conclusion

This paper presents a functional prototype for a versatile millimeter-scale tissue attachment mechanism, inspired by the terminal articulating array of curved hooks found in a tapeworm (*Taenia solium*) scolex. Through these efforts, we have demonstrated feasibility both in terms of the operating principle and manufacturability with a millimeter-scale prototype fabricated using laminate manufacturing techniques. We evaluated repeatable attachment to tissue-simulating surgical hydrogel blocks, with adhesion magnitude limited by the tissue phantom's tearing threshold, and not via failure of any component of the mechanism. This design is enabled by the addition of a steel sheet bending process, used to further expand the design space of laminate devices.

Future efforts to improve the performance of the device described in the present study could focus on several key areas, including: (i) mechanism miniaturization, e.g. through the incorporation of higher-strength adhesives to reduce delamination risk; (ii) on-demand controllable deployability and reversible anchoring, e.g. through the incorporation of alternative chemical, electrical, or magnetically coupled triggering systems; (iii) improved tissue adhesion strength, e.g. through modified hook morphology and linkage force transfer; (iv) improved biocompatibility through the incorporation of more environmentally stable materials or nonimmunogenic coatings; (v) exploration of actuator type and hook geometry; and (vi) the integration of our attachment mechanism into a functional ICR or other medical devices for monitoring, drug delivery, manipulation, sample collection, and related tasks.

Beyond device refinement, future parallel efforts could appreciably expand the device design space through a more exhaustive study of host–parasite interactions and novel geometric modifications for tissue- and habitat-specific anchoring strategies found across a broad range of parasitic taxa (cf. Fig. 1). While in the present study we have primarily focused on the development of tissue anchoring mechanisms for ICRs, the rich landscape of parasite adaptations (related to attachment, robustness, motility, etc.) is ripe for inspiring similar functionalities in other synthetic systems. The laminate manufacturing techniques described in this paper are uniquely well suited to functionally replicate many of these biological mechanisms and evaluate their potential in clinical applications. Despite the opportunities for device performance improvements in future iterations, the work presented

here highlights the great potential for the development of nonintuitive tissue-anchoring mechanisms using a combination of high-throughput lamination-based manufacturing strategies with detailed studies of parasitic biodiversity.

Materials and methods

Triggering test (Fig. 4C)

A block of Humimic Medical Gelatin #3 (Young's Modulus: 0.19 MPa) was placed on an Instron 100 N load-cell facing up (i.e. used as a scale) and plugged into the pull-tester. The device was then manually triggered by exerting increasing distributed pressure on the device until deployment occurred. Five separate force peaks that resulted in successful attachment were aligned and averaged.

Detachment test (Fig. 4D)

The detachment tests were conducted with a single-column Instron 5544A pull-tester with a 100 N load cell. The device was attached to a block of Humimic Medical Gelatin #3 (Young's Modulus: 0.19 MPa), and a normal force was applied until complete detachment had occurred. The force–displacement characteristics during detachment of four identical devices were evaluated. Three separate tests were conducted on each of the four devices ($n = 12$ total tests), with a new elastic element each time. The curves were aligned based on the detachment point and averaged.

High-speed triggering video

The high-speed triggering video was shot on a Phantom v1612 at 8,000 fps with an aperture time of 120 μs and an Extreme Dynamic Range setting of 60 μs. The contrast was then increased numerically in post processing to visualize the features of interest in more detail.

Scanning electron microscopy

All devices (in retracted and deployed configurations) were examined in their native state (uncoated) on a smooth, nontacky carbon substrate using a Tescan Vega GMU variable pressure scanning electron microscope.

Acknowledgments

The authors would like to acknowledge T. Geissenberger for help with the optical micrograph and E. Challita for assistance with the manuscript. Robert Wood holds stock in *Project* 1985, a surgical robotics company.

Supplementary Material

Supplementary material is available at *PNAS Nexus* online.

Funding

This material is based upon work supported by the National Science Foundation Graduate Research Fellowship under Grant No. 2140743. Any opinion, findings, and conclusions or recommendations expressed in this material are those of the authors and do not necessarily reflect the views of the National Science Foundation.

Author Contributions

Gabriel Maquignaz (Conceptualization, Formal analysis, Investigation, Methodology, Writing—original draft, Writing—review & editing), Rachel Zoll (Conceptualization, Formal analysis, Investigation, Methodology, Writing—original draft, Writing—review & editing), Michael Karpelson (Conceptualization, Investigation, Methodology), James C. Weaver (Conceptualization, Formal analysis, Investigation, Methodology, Writing—original draft, Writing—review & editing), and Robert J. Wood (Supervision, Funding acquisition, Writing—review & editing).

Data Availability

The data obtained from the experiment sessions are available at (84). The CAD files can be made available upon reasonable request.

References

1 Mau MM, Sarker S, Terry BS. 2021 Aug. Ingestible devices for long-term gastrointestinal residency: a review. *Prog Biomed Eng*. 3(4):042001. doi: 10.1088/2516-1091/ac1731.
2 Dickson I. 2018 Jan. Gas-sensing gut capsules. *Nat Rev Gastroenterol Hepatol*. 15(3):131–131. doi: 10.1038/NRGASTRO.2018.3.
3 Hafezi H, *et al.* 2015 Jan. An ingestible sensor for measuring medication adherence. *IEEE Trans Bio-med Eng*. 62(1):99–109. doi: 10.1109/TBME.2014.2341272.
4 Seong KY, *et al.* 2017 Nov. A self-adherent, bullet-shaped microneedle patch for controlled transdermal delivery of insulin. *J Control Release*. 265:48–56. doi: 10.1016/J.JCONREL.2017.03.041.
5 Munoz F, Alici G, Li W. 2014 May. A review of drug delivery systems for capsule endoscopy. *Adv Drug Deliv Rev*. 71:77–85. doi: 10.1016/J.ADDR.2013.12.007.
6 Abramson A, *et al.* 2020 Aug. Ingestible transiently anchoring electronics for microstimulation and conductive signaling. *Sci Adv*. 6(35). doi: 10.1126/sciadv.aaz0127.
7 Nan K, *et al.* 2024 Aug. An ingestible, battery-free, tissue-adhering robotic interface for non-invasive and chronic electrostimulation of the gut. *Nat Commun*. 15(1):1–12. doi: 10.1038/S41467-024-51102-5.
8 Roh Y, *et al.* 2021 Oct. Vital signal sensing and manipulation of a microscale organ with a multifunctional soft gripper. *Sci Rob*. 6(59). doi: 10.1126/scirobotics.abi6774.
9 Liu W, *et al.* 2024 Aug. Untethered microgrippers for biopsy in the upper urinary tract. *Adv Healthc Mater*. n/a(n/a):2401407. doi: 10.1002/adhm.202401407.
10 Han AK, Hajj-Ahmad A, Cutkosky MR. 2021 Feb. Hybrid electrostatic and gecko-inspired gripping pads for manipulating bulky, non-smooth items. *Smart Mater Struct*. 30(2):025010. doi: 10.1088/1361-665X/abca51.
11 Kaidarova A, *et al.* 2023 Sep. Wearable sensors for monitoring marine environments and their inhabitants. *Nat Biotechnol*. 41(9):1208–1220. doi: 10.1038/S41587-023-01827-3.
12 Fiorello I, *et al.* 2020 Sep. Climbing plant-inspired micropatterned devices for reversible attachment. *Adv Funct Mater*. 30(38):2003380. doi: 10.1002/ADFM.202003380.
13 Cummins G. 2021 Oct. Smart pills for gastrointestinal diagnostics and therapy. *Adv Drug Deliv Rev*. 177:113931. doi: 10.1016/j.addr.2021.113931.
14 Liu X, *et al.* 2019 Jan. Ingestible hydrogel device. *Nat Commun*. 10(1). doi: 10.1038/s41467-019-08355-2.

15 Toennies JL, Tortora G, Simi M, Valdastri P, Webster RJ. 2010 Jul. Swallowable medical devices for diagnosis and surgery: the state of the art. *Proc Inst Mech Eng Part C: J Mech Eng Sci*. 224(7): 1397–1414. doi: 10.1243/09544062JMES1879.

16 Tognarelli S, *et al.* 2009 Sep. Innovative stopping mechanism for esophageal wireless capsular endoscopy. *Procedia Chem*. 1(1): 485–488. doi: 10.1016/j.proche.2009.07.121.

17 Kong YL, *et al.* 2019. 3D-printed gastric resident electronics. *Adv Mater Technol*. 4(3):1800490. doi: 10.1002/admt.201800490.

18 Bellinger AM, *et al.* 2016 Nov. Oral, ultra-long-lasting drug delivery: application toward malaria elimination goals. *Sci Trans Med*. 8(365). doi: 10.1126/scitranslmed.aag2374.

19 Kirtane AR, *et al.* 2018 Jan. Development of an oral once-weekly drug delivery system for HIV antiretroviral therapy. *Nat Commun*. 9(1). doi: 10.1038/s41467-017-02294-6.

20 Kirtane AR, *et al.* 2019 Dec. A once-a-month oral contraceptive. *Sci Trans Med*. 11(521). doi: 10.1126/scitranslmed.aay2602.

21 Yim S, Sitti M. 2012 Feb. Design and rolling locomotion of a magnetically actuated soft capsule endoscope. *IEEE Trans Rob*. 28(1): 183–194. doi: 10.1109/tro.2011.2163861.

22 Yim S, Sitti M. 2012 Oct. Shape-programmable soft capsule robots for semi-implantable drug delivery. *IEEE Trans Rob*. 28(5): 1198–1202. doi: 10.1109/tro.2012.2197309.

23 Yim S, Goyal K, Sitti M. 2013 Aug. Magnetically actuated soft capsule with the multimodal drug release function. *IEEE ASME Trans Mechatron*. 18(4):1413–1418. doi: 10.1109/tmech.2012.2235077.

24 Yim S, Gultepe E, Gracias DH, Sitti M. 2014 Feb. Biopsy using a magnetic capsule endoscope carrying, releasing, and retrieving untethered microgrippers. *IEEE Trans Biomed Eng*. 61(2):513–521. doi: 10.1109/tbme.2013.2283369.

25 Abramson A, *et al.* 2019 Feb. An ingestible self-orienting system for oral delivery of macromolecules. *Science*. 363(6427):611–615. doi: 10.1126/science.aau2277.

26 Soon RH, *et al.* 2022 Aug. On-demand anchoring of wireless soft miniature robots on soft surfaces. *Proc Natl Acad Sci U S A*. 119(34):e2207767119. doi: 10.1073/PNAS.2207767119/SUPPL_FILE/PNAS.2207767119.SM04.MP4.

27 Zhang S, *et al.* 2015 Jul. A pH-responsive supramolecular polymer gel as an enteric elastomer for use in gastric devices. *Nat Mater*. 14(10):1065–1071. doi: 10.1038/nmat4355.

28 Do TN, En T, Seah T, Yu HK, Phee SJ. 2016 Jan. Development and testing of a magnetically actuated capsule endoscopy for obesity treatment. *PLoS One*. 11(1):e0148035. doi: 10.1371/journal.pone.0148035.

29 Kencana AP, *et al.* 2010. An ingestible wireless capsule for treatment of obesity. In: 2010 Annual International Conference of the IEEE Engineering in Medicine and Biology. p. 963–966. doi: 10.1109/IEMBS.2010.5627585.

30 Sarker S, Wankum B, Shimizu J, Jones R, Terry B. 2022. A factorial approach for optimizing the design parameters of a tissue attachment mechanism for drug delivery. *IEEE Trans Biomed Eng*. 69(1):32–41. doi: 10.1109/TBME.2021.3086975.

31 Sarker S, *et al.* 2022. A novel capsule-delivered enteric drug-injection device for delivery of systemic biologics: a pilot study in a porcine model. *IEEE Trans Biomed Eng*. 69(6): 1870–1879. doi: 10.1109/TBME.2021.3129653.

32 Yang X, Terry BS. 2013 Jun. An anchoring mechanism used to implant a biosensor in the small intestine. In: *Volume 1A: Abdominal Aortic Aneurysms; Active and Reactive Soft Matter; Atherosclerosis; BioFluid Mechanics; Education; Biotransport Phenomena; Bone, Joint and Spine Mechanics; Brain Injury; Cardiac Mechanics; Cardiovascular Devices, Fluids and Imaging; Cartilage and Disc Mechanics; Cell and Tissue Engineering; Cerebral Aneurysms; Computational Biofluid Dynamics; Device Design, Human Dynamics, and Rehabilitation; Drug Delivery and Disease Treatment; Engineered Cellular Environments*. American Society of Mechanical Engineers. doi: 10.1115/sbc2013-14807.

33 Tsubaki AT, Lewis WM, Terry BS. 2014 Jul. Implantation and carrier mechanism for long-term biosensing in the small intestine1. *J Med Devices*. 8(3). doi: 10.1115/1.4027124.

34 Xie W, Kothari V, Terry BS. 2015 Jun. A bio-inspired attachment mechanism for long-term adhesion to the small intestine. *Biomed Microdevices*. 17(4). doi: 10.1007/s10544-015-9972-7.

35 Xie W, *et al.* 2017 Jun. Design and validation of a biosensor implantation capsule robot. *J Biomech Eng*. 139(8). doi: 10.1115/1.4036607.

36 Song S, *et al.* 2022 Oct. Integrated design and decoupled control of anchoring and drug release for wireless capsule robots. *IEEE ASME Trans Mechatron*. 27(5):2897–2907. doi: 10.1109/tmech.2021.3125673.

37 Cheung E, Karagozler ME, Park S, Kim B, Sitti M. 2005. A new endoscopic microcapsule robot using beetle inspired microfibrillar adhesives. In: Proceedings, 2005 IEEE/ASME International Conference on Advanced Intelligent Mechatronics. IEEE. p. 551–557. doi: 10.1109/AIM.2005.1511040.

38 Glass P, Cheung E, Sitti M. 2008. A legged anchoring mechanism for capsule endoscopes using micropatterned adhesives. *IEEE Trans Biomed Eng*. 55(12):2759–2767. doi: 10.1109/TBME.2008.2002111.

39 Woo SH, Kim TW, Cho JH. 2009 Nov. Stopping mechanism for capsule endoscope using electrical stimulus. *Med Biol Eng Comput*. 48(1):97–102. doi: 10.1007/s11517-009-0553-x.

40 Zhou H, Alici G. 2019 Jun. A novel magnetic anchoring system for wireless capsule endoscopes operating within the gastrointestinal tract. *IEEE ASME Trans Mechatron*. 24(3):1106–1116. doi: 10.1109/tmech.2019.2909288.

41 Ghosh A, *et al.* 2020 Oct. Gastrointestinal-resident, shape-changing microdevices extend drug release in vivo. *Sci Adv*. 6(44). doi: 10.1126/sciadv.abb4133.

42 Chen Z, *et al.* 2024 Jan. A magnetic multi-layer soft robot for on-demand targeted adhesion. *Nat Commun*. 15(1):644. doi: 10.1038/s41467-024-44995-9.

43 Baik S, *et al.* 2019 Feb. Bioinspired adhesive architectures: from skin patch to integrated bioelectronics. *Adv Mater*. 31(34): 1803309. doi: 10.1002/adma.201803309.

44 Mahdavi A, *et al.* 2008 Feb. A biodegradable and biocompatible gecko-inspired tissue adhesive. *Proc Natl Acad Sci U S A*. 105(7): 2307–2312. doi: 10.1073/pnas.0712117105.

45 Surface HA. 1897. The lampreys of central New York. In: *Bulletin of the United States fish commission. Vol. 17. Washington, DC: Government Printing Office*. p. 209–215.

46 Wilson CB. 1902. North American parasitic copepods of the family argulidae, with a bibliography of the group and a systematic review of all known species. *Proc U. S. Natl Mus*. 25(1302): 635–742. doi: 10.5479/SI.00963801.25-1302.635.

47 Grundy JH. 1981. *Arthropods of medical importance*. Noble Books.

48 Bonnet S, Boulanger N. 2017 Jan. Ixodes tick saliva: a potent controller at the skin interface of early borrelia Burgdorferi sensu Lato transmission. In: *Arthropod vector: controller of disease transmission*. Vol. 2. Academic Press. p. 231–248. doi: 10.1016/B978-0-12-805360-7.00013-7.

49 Lebedeva D, Zietara M, Mendsaikhan B, Ermolenko A, Lumme J. 2023 Jul. Survivors from a pliocene climatic catastrophe: gyrodactylus (platyhelminthes, monogenea) parasites of the relict fishes in the central asian internal drainage basin of Mongolia. *Diversity (Basel)*. 15(7):860. doi: 10.3390/D15070860/S1.

50 Kumar K, *et al.* 2017 Dec. A biologically inspired, functionally graded end effector for soft robotics applications. *Soft Robo.* 4(4):317–323. doi: 10.1089/SORO.2017.0002.

51 Marquardt W, Demaree R. 1985. *Parasitology*. Macmillan.

52 Lisitsyna O. 2019 Aug. Fauna of Ukraine. Vol. 31. Acanthocephala.

53 Coleman GM, Beveridge I, Campbell RA. 2019 Jan. New species of Rhinebothrium Linton, 1890 (Cestoda: Rhinebothriidea) parasitic in Australian stingrays (Elasmobranchii: Batoidea). *Syst Parasitol.* 96(1):23–49. doi: 10.1007/S11230-018-9835-8.

54 Gorb SN. 2008 May. Biological attachment devices: exploring nature's diversity for biomimetics. *Philos Trans R Soc A: Math Phys Eng Sci.* 366(1870):1557–1574. doi: 10.1098/RSTA.2007.2172.

55 Lafferty KD, Kuris AM. 2002 Nov. Trophic strategies, animal diversity and body size. *Trends Ecol Evol.* 17(11):507–513. doi: 10.1016/S0169-5347(02)02615-0.

56 Poulin R, Keeney DB. 2008 Jan. Host specificity under molecular and experimental scrutiny. *Trends Parasitol.* 24(1):24–28. doi: 10.1016/j.pt.2007.10.002.

57 Baillie C, *et al.* 2019 Nov. Hooked on you: shape of attachment structures in cymothoid isopods reflects parasitic strategy. *BMC Evol Biol.* 19(1):1–11. doi: 10.1186/S12862-019-1533-X/TABLES/3.

58 Yang SY, *et al.* 2013 Apr. A bio-inspired swellable microneedle adhesive for mechanical interlocking with tissue. *Nat Commun.* 4(1). doi: 10.1038/ncomms2715.

59 Pritt B. 2016 Nov. Taenia Solium, scolex. http://parasitewonders.com/posts/post/taenia-solium-scolex.

60 Williams CF, Reading AJ, Scholz T, Shinn AP. 2011 Jan. Larval gryporhynchid tapeworms (Cestoda: Cyclophyllidea) of British freshwater fish, with a description of the pathology caused by Paradilepis scolecina. *J Helminthol.* 86(1):1–9. doi: 10.1017/s0022149x10000866.

61 Mahvash M, Dupont PE. 2010 Apr. Mechanics of dynamic needle insertion into a biological material. *IEEE Trans Biomed Eng.* 57(4):934–943. doi: 10.1109/TBME.2009.2036856.

62 Whitney JP, Sreetharan PS, Ma KY, Wood RJ. 2011 Oct. Pop-up book MEMS. *J Micromech Microeng.* 21(11):115021. doi: 10.1088/0960-1317/21/11/115021.

63 Sreetharan PS, Whitney JP, Strauss MD, Wood RJ. 2012 Apr. Monolithic fabrication of millimeter-scale machines. *J Micromech Microeng.* 22(5):055027. doi: 10.1088/0960-1317/22/5/055027.

64 Gafford JB, Kesner SB, Wood RJ, Walsh CJ. 2013 Aug. Microsurgical devices by pop-up book MEMS. In: Volume 6A: 37th mechanisms and robotics conference. American Society of Mechanical Engineers. doi: 10.1115/detc2013-13086.

65 Gafford J, *et al.* 2017 Jan. Toward medical devices with integrated mechanisms, sensors, and actuators via printed-circuit MEMS. *J Med Devices.* 11(1). doi: 10.1115/1.4035375.

66 Uicker JJ, Pennock GR, Shigley JE. 2017. *Theory of machines and mechanisms*. 5th ed. New York: Oxford University Press.

67 Ding X, Kong X, Dai JS. 2016. *Advances in reconfigurable mechanisms and robots II, volume 36 of Mechanisms and machine science*. Cham: Springer International Publishing. doi: 10.1007/978-3-319-23327-7.

68 Serrano FR, Steinhardt E, Wood RJ. 2024. Considerations for the design and rapid manufacturing of pop-up MEMS devices. *Adv Mater Technol.* 9(8):2301940. doi: 10.1002/admt.202301940.

69 Tran S, *et al.* 2023 Jul. Development of an optically transparent kidney model for laser lithotripsy research. *BJU Int.* 132(1):36. doi: 10.1111/BJU.16015.

70 Laughlin ME, Stephens SE, Hestekin JA, Jensen MO. 2022 Feb. Development of custom wall-less cardiovascular flow phantoms with tissue-mimicking gel. *Cardiovasc Eng Technol.* 13(1):1–13. doi: 10.1007/S13239-021-00546-7/FIGURES/10.

71 Ling J, *et al.* 2017 Apr. Effect of honeybee stinger and its microstructured barbs on insertion and pull force. *J Mech Behav Biomed Mater.* 68:173–179. doi: 10.1016/j.jmbbm.2017.01.040.

72 Kurniawan N, Keuchel M. 2014. Technology. In: *Video capsule endoscopy*. Berlin, Heidelberg: Springer. p. 15–20. doi: 10.1007/978-3-662-44062-9_3.

73 McAlindon ME, Hagenmüller F, Fleischer DE. 2014. Fields of application. In: *Video capsule endoscopy*. Berlin Heidelberg: Springer. p. 5–13. doi: 10.1007/978-3-662-44062-9_2.

74 Wang J, *et al.* 2017 Sep. Capsule ultrasound device: characterization and testing results. In: 2017 IEEE International Ultrasonics Symposium (IUS). IEEE. doi: 10.1109/ultsym.2017.8092071.

75 Lee JH, Traverso G, Ibarra-Zarate D, Boning DS, Anthony BW. 2020 Mar. Ex vivo and in vivo imaging study of ultrasound capsule endoscopy. *J Med Devices.* 14(2). doi: 10.1115/1.4046352.

76 Steinberg WH, Mina FA, Pick PG, Frey GH. 1965 May. Heidelberg capsule I. *J Pharm Sci.* 54(5):772–776. doi: 10.1002/jps.2600540522.

77 Farmer AD, Scott SM, Hobson AR. 2013 Dec. Gastrointestinal motility revisited: the wireless motility capsule. *United Eur Gastroenterol J.* 1(6):413–421. doi: 10.1177/2050640613510161.

78 Saad RJ, Hasler WL. 2011 Dec. A technical review and clinical assessment of the wireless motility capsule. *Gastroenterol Hepatol (N Y).* 7(12):795–804.

79 Li P, Kreikemeier-Bower C, Xie W, Kothari V, Terry BS. 2017 Mar. Design of a wireless medical capsule for measuring the contact pressure between a capsule and the small intestine. *J Biomech Eng.* 139(5). doi: 10.1115/1.4036260.

80 Kalantar-Zadeh K, *et al.* 2018 Jan. A human pilot trial of ingestible electronic capsules capable of sensing different gases in the gut. *Nat Electron.* 1(1):79–87. doi: 10.1038/s41928-017-0004-x.

81 Singh S, *et al.* 2019 May. Sa1717 – development of a swallowable diganostic capsule to monitor gastrointestinal health. *Gastroenterology.* 156(6):S–376. doi: 10.1016/s0016-5085(19)37784-4.

82 Yoo E-H, Lee S-Y. 2010 May. Glucose biosensors: an overview of use in clinical practice. *Sensors.* 10(5):4558–4576. doi: 10.3390/s100504558.

83 Mitragotri S, Burke PA, Langer R. 2014 Aug. Overcoming the challenges in administering biopharmaceuticals: formulation and delivery strategies. *Nat Rev Drug Discov.* 13(9):655–672. doi: 10.1038/nrd4363.

84 Maquignaz G, Zoll R. 2024. doi: Design and fabrication of a parasite inspired millimeter scale tissue anchoring mechanism. https://github.com/harvard-microrobotics/parasite-attachment-mechanism.